

Applications of artificial intelligence in the analysis of histopathology images of gliomas: a review

Jan-Philipp Redlich^{1,*}, Friedrich Feuerhake^{2,3}, Joachim Weis⁴, Nadine S. Schaadt², Sarah Teuber-Hanselmann⁵, Christoph Buck⁶, Sabine Luttmann⁷, Andrea Eberle⁷, Stefan Nikolin⁴, Arno Appenzeller⁸, Andreas Portmann⁹, André Homeyer¹

¹Fraunhofer Institute for Digital Medicine MEVIS, Max-von-Laue-Straße 2, 28359 Bremen, Germany

²Hannover Medical School, Carl-Neuberg-Straße 1, 30625 Hannover, Germany

³Institute of Neuropathology, Medical Center - University of Freiburg, Breisacherstraße 64, 79106 Freiburg, Germany

⁴Institute of Neuropathology, RWTH Aachen University Hospital, Pauwelsstrasse 30, 52074 Aachen, Germany

⁵Department of Neuropathology, Center for Pathology, Klinikum Bremen-Mitte, Sankt-Jürgen-Straße 1, 28205 Bremen, Germany

⁶Leibniz Institute for Prevention Research and Epidemiology - BIPS, Achterstraße 30, 28359 Bremen, Germany

⁷Bremen Cancer Registry, Leibniz Institute for Prevention Research and Epidemiology - BIPS, Achterstraße 30, 28359 Bremen, Germany

⁸Fraunhofer Institute of Optronics, System Technologies and Image Exploitation IOSB, Fraunhoferstraße 1, 76131 Karlsruhe, Germany

⁹German Heart Center Berlin, Augustenburger Platz 1, 13353 Berlin, Germany

*Corresponding author. E-mail address: jan-philipp.redlich@mevis.fraunhofer.de

Abstract

In recent years, the diagnosis of gliomas has become increasingly complex. Analysis of glioma histopathology images using artificial intelligence (AI) offers new opportunities to support diagnosis and outcome prediction. To give an overview of the current state of research, this review examines 70 publicly available research studies that have proposed AI-based methods for whole-slide histopathology images of human gliomas, covering the diagnostic tasks of subtyping (16/70), grading (23/70), molecular marker prediction (13/70), and survival prediction (27/70). All studies were reviewed with regard to methodological aspects as well as clinical applicability. It was found that the focus of current research is the assessment of hematoxylin and eosin-stained tissue sections of adult-type diffuse gliomas. The majority of studies (49/70) are based on the publicly available glioblastoma and low-grade glioma datasets from The Cancer Genome Atlas (TCGA) and only a few studies employed other datasets in isolation (10/70) or in addition to the TCGA datasets (11/70). Current approaches mostly rely on convolutional neural networks (53/70) for analyzing tissue at 20x magnification (30/70). A new field of research is the integration of clinical data, omics data, or magnetic resonance imaging (27/70). So far, AI-based methods have achieved promising results, but are not yet used in real clinical settings. Future work should focus on

the independent validation of methods on larger, multi-site datasets with high-quality and up-to-date clinical and molecular pathology annotations to demonstrate routine applicability.

Introduction

Gliomas account for roughly a quarter of all primary non-malignant and malignant central nervous system (CNS) tumors, and 81% of all malignant primary CNS tumors¹. Generally, gliomas can be differentiated into circumscribed and diffuse gliomas^{2,3}. Whereas circumscribed gliomas are usually benign and potentially curable with complete surgical resection, diffuse gliomas are characterized by a diffuse infiltration of tumor cells in the brain parenchyma and are mostly not curable, with an inherent tendency for malignant progression and recurrence^{2,3}. In particular, glioblastoma, the most common and most aggressive malignant CNS tumor, makes up 60% of all diagnosed gliomas and caused 131,036 deaths in the US between 2001 and 2019 alone¹. Although the introduction of now well-established standard therapy protocols involving surgical resection, radiation and chemotherapy⁴ as well as guidance by MGMT promoter methylation status⁵ has substantially improved clinical outcomes, 5-year survival in patients with glioblastoma has been largely constant at only 6.9%¹.

The current international standard for the diagnosis of gliomas is the fifth edition of the WHO Classification of Tumors of the Central Nervous System, published in 2021⁶. Based on advances in the understanding of CNS tumors, the WHO classification system has been constantly evolving since its first issue in 1979, with new versions released every 7–9 years⁷. Whereas previous versions greatly relied on histological assessment via light microscopy, the current classification system incorporates both histopathological features and molecular alterations (Figure 1), allowing for a more uniform delineation of disease entities^{6,7}. The basic principle of classification according to histological typing, histogenesis, and grading, however, remains fundamental and underlines the role of conventional histological assessment as an important element of timely, standardized, and globally consistent diagnostic workflows⁶.

The rapidly evolving field of computational pathology, in particular, the analysis of digital whole-slide images (WSIs) of tumor tissue sections using artificial intelligence (AI), offers new opportunities to support current diagnostic workflows. Promising applications range from automation of time-consuming routine tasks, such as subtyping and grading, to tasks that cannot be accurately performed by human observers, such as predicting molecular markers or survival directly from hematoxylin and eosin (H&E)-stained routine sections of formalin-fixed and paraffin-embedded (FFPE) tumor tissue^{8,9}. Key concepts of AI-based analysis of WSIs are briefly explained in Box 1.

Motivated by a significant increase in corresponding publications in recent years (Figure 2), this review provides a comprehensive overview of the current state of research on AI-based analysis, including both traditional machine learning (ML) and deep learning (DL), of whole-slide histopathology images of human gliomas. Whereas prior related reviews on AI-based glioma assessment focused on magnetic resonance imaging (MRI)^{10–13} and specific tasks, such as grading^{14,15} or survival prediction^{16–18}, this review focuses specifically on the histological assessment of gliomas and covers the tasks of subtyping, grading, molecular marker prediction, and survival prediction. The reviewed studies are examined

with regard to diagnostic tasks and methodological aspects of WSI processing, as well as discussed by addressing limitations and future directions. Studies primarily investigating segmentation¹⁹, tumor heterogeneity^{20,21}, or image retrieval²² have been considered out of scope.

Methods

Literature search was last updated on 02.06.2023, and conducted as follows: PubMed and Google Scholar were searched using the search term “(glioma OR glioblastoma OR brain tumor) AND (computational pathology OR machine learning OR deep learning OR artificial intelligence) AND (whole slide image OR WSI)”. All 72 and the first 200 search results from PubMed and Google Scholar, respectively, were identified for further consideration. The criteria for inclusion in this review required that the studies have proposed AI-based methods for whole-slide histopathology images of confirmed human glioma cases that cover the diagnostic tasks of subtyping, grading, molecular marker prediction, or survival prediction. A total of 70 studies, comprising journal articles, conference contributions and preprints, were included in this review. In the case of conference contributions and preprints that were subsequently published as journal articles, only the latter were considered.

Results

Diagnostic tasks

The reviewed body of research comprises 70 studies that have proposed AI-based methods for whole-slide histopathology images of confirmed human glioma cases. The studies covered the diagnostic tasks of subtyping (16/70), grading (23/70), molecular marker prediction (13/70), and survival prediction (27/70). All studies focused on the assessment of adult-type diffuse gliomas (Figure 1) based on H&E-stained tissue sections (one exception incorporated immunohistochemistry (IHC) staining²³).

The majority of the studies (49/70) were based on two public datasets from The Cancer Genome Atlas, namely from the Glioblastoma^{24,25} (TCGA-GBM) and Low-Grade Glioma²⁶ (TCGA-LGG) projects. Both contain information on diagnosis, molecular alterations, and survival for roughly 600 and 500 patients, respectively. Patients in both datasets had been diagnosed before 2013 and 2011^{24–26} and therefore according to versions of the WHO classification system prior to 2016. The TCGA-GBM dataset includes primary glioblastomas, WHO grade IV, and the TCGA-LGG dataset includes astrocytomas, anaplastic astrocytomas, oligodendrogliomas, oligoastrocytomas, and anaplastic oligoastrocytomas, all WHO grade II or III.

Other studies employed other datasets in isolation (10/70) or in addition to the TCGA datasets (11/70). Diagnoses in these datasets corresponded either to versions of the WHO classification from 2016^{27–30} or earlier^{31,32}.

It should be noted that the 2021 WHO Classification of Tumors of the Central Nervous System changed the notation of tumor grades from roman to arabic numerals and endorses the use of the term “CNS WHO grade”⁶. Throughout this review, these changes in notation are used only for diagnoses which were reported according to the WHO classification system from 2021.

Subtyping

Subtyping gliomas is of fundamental importance for the diagnostic workup and subsequent patient management^{6,7}. Before 2016, the WHO classification system incorporated only histological features. Oligodendrogliomas, for instance, were characterized by features including round nuclei and a “fried egg” cellular appearance; astrocytomas by more irregular nuclei with clumped chromatin, eosinophilic cytoplasm and branched cytoplasmic processes; and glioblastomas by an astrocytic phenotype combined with the presence of necrosis and/or microvascular proliferation⁷. The latest revisions of the WHO classification system published in 2016 and 2021 reflect important advances in the understanding of the molecular pathogenesis of gliomas by incorporating molecular alterations in an integrated diagnosis (Figure 1). For instance, since 2021, the diagnosis of glioblastoma has been limited to malignant non-IDH-mutated (i.e., IDH-wildtype) gliomas. Oligoastrocytomas which until 2016 were considered a separate tumor entity with mixed oligodendroglial and astrocytic histological features, could between 2016 and 2021 only be diagnosed in cases with unknown 1p/19q and IDH status (designated as “oligoastrocytoma, NOS (Not Otherwise Specified)”, and not recommended unless molecular testing was unavailable). Since 2021, oligoastrocytomas are no longer considered^{6,7}. Table 1 provides an overview of all corresponding studies grouped according to the investigated subtyping tasks.

Most studies predicted glioma type from WSIs of H&E-stained tissue sections in an end-to-end manner, i.e., without prior identification of pre-defined histological or molecular markers. Two exceptions from this, include one study that inferred subtypes from predictions for necrosis and microvascular proliferation, IDH mutation, 1p/19q codeletion, and homozygous deletion of CDKN2A/B³³; and another study that aligned IHC- (for IDH1-R132H and ATRX) and H&E-stained tissue sections to differentiate along IDH mutation status and astrocytic lineage²³.

Approaches based on weakly-supervised learning (WSL), in which predictions of patch-level convolutional neural networks (CNNs) were aggregated to patient-level diagnosis, were commonly employed^{27,30,34,35}. Aggregation in these approaches was based on majority voting^{30,35} or on traditional ML methods fitted to histograms of patch-level predictions^{27,34}. Most recently, Shi et al. (2023) proposed two such models for diagnosing intracranial germinomas, oligodendrogliomas, and low-grade astrocytomas from H&E-stained and intraoperative frozen sections, respectively³⁰. They compared the diagnostic accuracy of three pathologists with and without the assistance of their proposed models and reported an average improvement of 40% and 20%, respectively.

Two recent approaches leveraged Vision Transformers (ViTs)^{29,33}. Most notably, Li et al. (2023), employed TCGA data and a proprietary patient cohort for three tasks of brain tumor classification, including glioma subtyping, as well as prediction of IDH1, TP53, and MGMT status in gliomas²⁹. Their proposed model featured an ImageNet pre-trained ViT for encoding image patches and a graph- and Transformer-based aggregator for modeling relations

among patches. It achieved high performance in all tasks and automatically learned histopathological features, including blood vessels, hemorrhage, calcification, and necrosis.

Numerous approaches that improved predictive performance for differentiating astrocytomas, oligodendrogliomas, and glioblastomas by integration of MRI (up to 7.8% in terms of balanced accuracy³⁶) emerged from the CPM-RadPath challenges held in 2018, 2019, and 2020. The best performing and subsequently published approaches^{36–38} utilized weakly-supervised CNNs (or an ensemble thereof³⁶) for processing WSIs and fused WSI- and MRI-derived predictions by an average pooling³⁶, a max pooling³⁷ or by favoring WSI-derived predictions³⁸.

Grading

Complementing tumor types, tumor grades differentiate gliomas according to predicted clinical behavior and range from CNS WHO grade 1 to 4, with CNS WHO grade 1 indicating the least malignant behavior^{2,6}. Similar to subtyping, grading is currently based on both histological and molecular markers (Figure 1), whereas in the past only histological markers, including cellular pleomorphism, proliferative activity, necrosis, and microvascular proliferation were considered⁷. Table 2 provides an overview of all corresponding studies grouped according to the investigated grading tasks.

All studies predicted grade from WSIs of H&E-stained tissue sections in an end-to-end manner, with the exception of one study that inferred grade from detected necrosis and microvascular proliferation³⁹.

Earlier studies mostly employed handcrafted features and traditional ML methods^{32,39–44}. In a typical study, Barker et al. (2016) propose a coarse-to-fine analysis based on handcrafted features derived from segmented nuclei to first select discriminative patches used for subsequent grading by means of a linear regression model⁴².

All other studies employed CNNs for predicting grade from image patches. Three such approaches decomposed II vs. III vs. IV grading as stepwise binary II and III vs. IV followed by II vs. III classifications and agreed on greater difficulty in differentiating grades II vs. III^{45–47}. Su et al. (2023) focused on this challenge and reported considerable performance by employing an ensemble of 14 weakly-supervised CNN classifiers whose predictions were aggregated by a logistic regression model⁴⁸. Whereas this approach seems computationally intensive, Momeni et al. (2018) proposed a deep recurrent attention model, although for II and III vs. IV grading, which achieved state-of-the-art results while only analyzing 144 image patches per WSI⁴⁹.

Several studies integrated additional modalities such as genomics^{45,50,51}, age and sex⁴¹ or proliferation index manually assessed from Ki-67 staining³². Most notably, Qiu et al. (2023) adopted a self-training strategy to address the effects of label noise and proposed an attention-based feature guidance aiming to capture bidirectional interactions between WSIs and genomic features⁵⁰. They demonstrated superiority of multi-modal over uni-modal predictions (AUC 0.807 (WSI), 0.804 (genomics), 0.872 (WSI+genomics)) as well as effectiveness of modeling bidirectional interactions between modalities for glioma grading and lung cancer subtyping.

Addressing the problem of possibly limited availability of genomics in clinical practice, Xing et al. (2022) proposed a knowledge distillation framework to transfer the privileged knowledge of a teacher model, trained on WSIs and genomics, to a student model which subsequently predicts grade solely from WSIs⁵². Remarkably, they report superior performance of their uni-modal student model over a state-of-the-art multi-modal model⁵¹ on the same validation cohort.

Molecular marker prediction

Molecular alterations in gliomas have diagnostic, predictive and prognostic value critical for effective treatment selection, e.g., the presence of MGMT promoter methylation was associated with a beneficial sensitivity to alkylating agent chemotherapy, resulting in prolonged survival in glioblastoma patients^{2,5}. Standards of practice for accurate, reliable detection of molecular markers include immunohistochemistry, sequencing or fluorescent in situ hybridization². Table 3 provides an overview of all corresponding studies grouped according to the investigated molecular markers.

Although there are no established criteria for determining molecular markers from histology yet, a growing body of research has suggested their predictability from WSIs of H&E-stained tissue sections with considerable accuracy. Among others, pan-cancer studies predicted various molecular markers across multiple cancer types^{53–55} and with regard to glioblastoma reported an externally validated accuracy of over 0.7 for 4 out of 9 investigated markers⁵³.

IDH mutation was investigated by all except one study, with similar approaches based on weakly-supervised CNNs augmented by either the incorporation of additional synthetically generated image patches (AUC 0.927 vs. 0.920)⁵⁶ or by the integration of MRI (ACC 0.860 (WSI), 0.780 (MRI), 0.900 (WSI+MRI))⁵⁷.

Patient age and IDH mutation status are highly correlated. For instance, the median age at diagnosis was reported to be 37 years for IDH-mutant astrocytomas and 65 years for IDH-wildtype astrocytomas¹. As such, integration of patient age into multi-modal predictions consistently improved performance^{56–58}.

Comparing their performance in predicting IDH status to pathologists, Liechty et al. (2022) proposed a multi-magnification ensemble that averaged predictions from multiple weakly-supervised CNN classifiers, each processing individual magnification levels⁵⁹. On an external validation cohort of 174 WSIs, their model did not surpass human performance (AUC 0.881 vs. 0.901), but averaged predictions from pathologists and their model performed on par with the consensus of two pathologists (AUC 0.921 vs. 0.920).

As various molecular markers show complex interactions and should not be considered as independent variables (e.g., “essentially all 1p/19q co-deleted tumours are also IDH-mutant, although the converse is not true”²), Wang et al. (2023) proposed a multiple-instance learning (MIL)- and ViT-based model for predicting IDH mutation, 1p/19q codeletion, and homozygous deletion of CDKN2A/B as well as the presence of necrosis and microvascular proliferation, while simultaneously recognizing interactions between predicted markers³³. They validated their system in ablation studies and outperformed popular state-of-the-art MIL frameworks and CNN architectures in all tasks, with improvements in accuracy of up to 6.3%.

Survival prediction

Accurate prediction of survival and comprehensive understanding of prognostic factors in gliomas are crucial for appropriate disease management⁶⁰. Median survival in adult-type diffuse gliomas ranges from 17 years in oligodendrogliomas to only 8 months in glioblastomas and generally decreases with older age¹. Besides type, grade and age, other prognostic factors include tumor size and location, extent of tumor resection, performance status, cognitive impairment, status of molecular markers such as IDH mutation, 1p/19q codeletion, MGMT promoter methylation and treatment protocols, including temozolomide and radiotherapy^{2,60}. Table 4 provides an overview of all corresponding studies grouped according to the investigated aspects of prognostic inference.

Almost all reviewed studies investigated the prediction of overall survival from WSIs of H&E-stained tissue sections in an end-to-end manner. One exception inferred predictions by first classifying vascular endothelial cells and quantifying microvascular hypertrophy and hyperplasia⁶¹ and two studies additionally investigated disease-free survival^{54,62}. Most studies predicted risk scores or survival times, and only four studies conducted survival prediction by classifying patients into either low- or high-risk groups^{63–65} or four predefined risk groups⁶⁶.

Given the high variability of disease manifestation and co-morbidities, as well as the stochastic nature of the immediate cause of death, prognosis can be regarded as the most challenging task. In particular, prediction of overall survival from histology has been considered inherently more challenging than tasks such as subtyping and grading^{51,67–70}, as complex interactions of heterogeneous visual concepts, such as immune cells in general⁷¹, or more specifically lymphocyte infiltrates⁷² in the tumor microenvironment, have been recognized as potentially relevant factors.

Zhu et al. (2017) proposed WSISA, the earliest end-to-end system for survival prediction from WSIs, which leveraged a priorly proposed CNN-based survival model⁷³ to first compute clusters of survival-discriminate image patches and second aggregate cluster-based features for subsequent risk score regression⁷⁰.

Potentially due to the aforementioned complexity, only a minority of the reviewed studies proposed uni-modal approaches based on handcrafted features or weakly-supervised CNNs. The majority of the studies utilized either more intricate architectures, or the integration of additional modalities of information

To this end, Li et al. (2018) and Chen et al. (2021) set out to capture context-aware representations of histological features by employing graph convolutional neural networks, in which vertices corresponded to patch-level feature vectors and edges were defined by either Euclidean distance between feature vectors or adjacency of patches^{74,75}. They both compared their models, DeepGraphSurv and Patch-GCN, respectively, on multiple cancer types, where DeepGraphSurv improved on WSISA by 6.5% and Patch-GCN on DeepGraphSurv by 2.6% in terms of C-index.

Three recent studies leveraged Transformer for modeling histological patterns across patches, either by employing multiple feature detectors to aggregate distinct morphological patterns^{68,76} or by fusing information from multiple magnification levels⁶⁷. All studies reported state-of-the-art performance on multiple cancer types, including gliomas, from the TCGA-GBM and TCGA-LGG datasets. Most notably, Liu et al. (2023) reported a 13.2% and

a 4.3% C-index performance improvement compared to DeepGraphSurv and Patch-GCN on TCGA-LGG, respectively, and Wang et al. (2023) reported a 5.5%, a 4.5%, and a 3.5% C-index performance improvement compared to DeepGraphSurv, Patch-GCN, and an extension of Patch-GCN via a variance pooling⁷⁷ on TCGA-GBM and TCGA-LGG^{67,68}.

Contrasting the abovementioned uni-modal approaches, half of all studies stated prognosis as a multi-modal problem by integrating clinical or omics data. Simple approaches to such integration included fusing WSI-derived risk scores and variables from other modalities in Cox proportional hazards models^{58,62,78} or by concatenating image features and variables prior to subsequent risk score prediction, as proposed by Mobadersany et al. (2018)⁷⁹. In particular, they proposed two CNN-based models, SCNN, which predicted survival from priorly delineated regions of interest (ROIs), and GSCNN, which improved SCNN by concatenating IDH mutation and 1p/19q codeletion status as additional prognostic variables (C-index 0.801 vs. 0.754). They further reported the superiority of concatenation vs. Cox models as strategies for multi-modal fusion (C-index 0.801 vs. 0.757).

More advanced approaches fused distinct uni-modal feature representations into an intermediate feature tensor, by means of the Kronecker product, while controlling the expressiveness of each modality via a gating-based attention mechanism^{51,80,81}. Most notably, by integrating 320 genomics and transcriptomics features in this manner, Chen et al. (2022) surpassed GSCNN on the same ROIs with a C-index performance improvement of 5.8%⁵¹. The same authors later expanded on this approach by adopting MIL applying it to 14 cancer types⁸⁰. They conducted extensive analysis regarding the interpretability of their model and reported that presence of necrosis and IDH1 mutation status were the most attributed features in gliomas from the TCGA-LGG dataset, which is in line with the current WHO classification. They further developed an interactive research tool, to drive the discovery of new prognostic biomarkers.

Methodological aspects of WSI processing

Across all diagnostic tasks, most of the considered studies processed WSIs in a patch-based manner. The predictive performance of such approaches depends on choices for patch size and magnification, methods for encoding image patches, and approaches for learning relations among patches. In the following, the studies are examined in more detail with regard to these aspects.

Patch sizes and magnifications

The size of image patches and the magnification at which they are extracted not only determine the number of patches stemming from given WSIs, but also influence the degree to which either cellular details or more distributed characteristics in tissue architecture are captured. However, patch size and magnification were not consistently reported (56/70 and 43/70, respectively) and only three studies compared performance across multiple sizes and magnifications, e.g., patches of size 256 x 256 pixels and 2.5x, 5x, 10x, and 20x magnification for IDH mutation prediction (AUC 0.80, 0.85, 0.88, and 0.84, respectively)⁵⁹; highest performance in grading by employing 672 x 672 pixels patches at 40x magnification⁸²; and highest performance for survival risk group classification consistent across multiple CNN architectures by utilizing 256 x 256 pixels patches at 20x

magnification⁶⁶. Apart from these comparisons, smaller patches, i.e., 224 x 224 and 256 x 256 pixels, and 20x magnification were most frequently employed (Figure 3).

In addition to single-magnification approaches, few studies processed multiple magnifications^{31,34,57,59,67,83}, e.g., by concatenating single-magnification features at the onset⁸³, averaging of single-magnification predictions⁵⁹ or modeling magnifications using graphs³¹ or cross-attention⁶⁷.

Encoding of image patches

The reviewed studies employed handcrafted features (13/70), CNNs (53/70), including ResNet⁸⁴, VGG⁸⁵, DenseNet⁸⁶, EfficientNet⁸⁷, Inception⁸⁸ and AlexNet⁸⁹, capsule networks (1/70), autoencoders (1/70) and ViTs (2/70) to encode image patches. While handcrafted features were mostly employed by earlier approaches, ViT emerged in recent years. Few studies compared different CNN architectures^{28,35,56,66} and mostly agreed on the superiority of ResNet over other popular architectures^{28,35,56}. Apart from these comparisons, ResNet architectures pre-trained on ImageNet were most commonly employed (29/53) (Figure 4). Self-supervised learning approaches for pre-training CNNs or ViTs using histopathological images leveraged pre-text tasks, including contrastive learning^{53,83,90–93}, masked pre-training⁹⁴ or cross-stain prediction⁹⁰.

Learning paradigms

Considering all 57 DL-based approaches, studies either employed previously delineated ROIs (11/57) or adopted WSL (22/57) or MIL (21/57). In recent years, MIL was most commonly used (Figure 5), and approaches mostly utilized ResNets for encoding image patches (14/21) as well as intricate architectures based on graphs^{74,75}, Transformers^{29,33,67–69,76,80,94,95} or other attention mechanisms^{31,53,63,90–92,96} (often combinations thereof) to model histological patterns among patches.

Few studies compared approaches but consistently reported the superiority of MIL over WSL^{29,33,53}. Most interestingly, Li et al. (2023) conducted insightful comparisons across three subtyping tasks and reported an overall superiority of ViT-L-16 over ResNet50 (both pre-trained on ImageNet) and a worse performance of WSL in all three tasks, with an especially large performance gap in a more fine-grained subtyping task including 11 brain tumor types²⁹.

Discussion

As described in the previous sections, a large body of research on the application of AI to various aspects of glioma tissue assessment has been published in recent years. Considering the difficulty of the diagnostic tasks, each study provides important insights for the future application of AI-based methods in real clinical settings. However, there still remain serious limitations.

Limitations of current research

Only seven of the included studies evaluated the performance of their proposed method on independent test datasets from external pathology departments that were not used during the development of the method^{29,30,42,53,54,59,66}. External validation, however, is crucial for meaningful performance estimates⁹⁷. Moreover, the performance metrics reported in the solely TCGA-based studies might be inflated, as none of these studies ensured that the data used for model development and performance estimation originated from distinct tissue source-sites^{98,99}. As the TCGA datasets were originally compiled for different purposes^{24–26}, it must be assumed that they are not representative of the intended use of the proposed analysis methods and contain biases. Given these limitations, the performance metrics reported by the reviewed studies should be interpreted with caution and should not be generalized to practical applications¹⁰⁰.

Relatedly, all TCGA-based studies utilized different subpopulations of the two TCGA cohorts without specifying which selection criteria were employed. When studies used other datasets, these were generally not made publicly available. This makes it very hard to reproduce the results and compare results between studies.

Another important aspect is the repeated revision of the WHO classification system, which makes it necessary to revise the now outdated ground truth labels in the TCGA datasets with the current subtypes and grades. Only two studies made an effort to reclassify the TCGA cohorts according to the current 2021 criteria based on available molecular information^{33,35}, and only four studies considered the previous version from 2016^{28–31}. All other studies were based on versions from 2007 or earlier, which seriously limits their comparability with the current diagnostic standards, and largely disregards important advances in the understanding of glioma tumor biology. Notably, this concerns important advances regarding the molecular pathogenesis of gliomas with an impact on classification and prognostication, as reflected by the revisions from 2016 and 2021^{6,7}.

A commonality of many studies in the field is their emphasis on technical aspects of AI approaches, with less focus on the clinical applicability of their proposed methods. The design of a number of studies suggests that the investigations were primarily based on availability of data, while a clearly defined clinically relevant research question was not immediately apparent. Examples include studies that mixed distinct glioma types and grades without properly substantiating the motivation for their respective approaches, for instance, when differentiating patients in the TCGA-GBM cohort from those in the TCGA-LGG cohort^{34,40–44,49,94,101,102}. Moreover, not all studies accurately specified if FFPE or frozen sections were considered for histological assessment. In many studies, it remained unclear for which specific practical diagnostic tasks the proposed methods were envisioned to be relevant.

Future directions

Considering that the majority of currently available research results are based largely on data from the public TCGA-GBM and TCGA-LGG projects, the acquisition of new datasets with high-quality and up-to-date clinical and molecular pathology annotations is of utmost importance to progress towards clinical applicability. Such new datasets should address the

aforementioned limitations, that is, they should consider the latest version of the WHO classification system, be representative of the intended use¹⁰⁰, and include multiple tissue source sites to enable independent external validation⁹⁷. Moreover, depending on the intended use cases, the value of such datasets would increase with extension to additional glioma types beyond adult-type diffuse gliomas, or additional tissue staining modalities on top of H&E.

Regarding multi-modal fusion, all studies, across all diagnostic tasks, reported better predictive performance when clinical data, omics data, MRI and WSIs were used in combination rather than individually. So far, the additional value of WSIs for multi-modal predictive performance has been consistently low^{51,62,63,80,103}. Moreover, good predictive performance can often be achieved with much simpler models. For instance, Cox proportional hazards or logistic regression models based on a few clinical variables, such as patient age and sex, can perform on par with WSI-based predictions for survival or IDH mutation status^{51,58,78–80,104}. Further research should therefore be conducted to better understand and improve the added value of AI-based analysis of WSIs for glioma.

Above all, the reviewed literature clearly indicates a need for future studies with a stronger focus on clinically relevant scientific questions. This requires a truly interdisciplinary approach from the outset, involving neuropathology, neuro-oncology, and the broad expertise of computational science and medical statistics.

Data availability

The authors declare that the main data supporting the findings of this study are available within this manuscript.

Acknowledgements

Research reported in this publication was supported by the German Federal Ministry of Health based on a resolution of the German Bundestag (funding codes: ZMI5-2522DAT15A, ZMI5-2522DAT15B, ZMI5-2522DAT15C, ZMI5-2522DAT15D, ZMI5-2522DAT15E). FF received additional funding from ERACoSysMed and the German Federal Ministry of Education and Research (BMBF) under grant number FKZ 31L0237A (MiEDGE).

Author contributions

JPR and AH conceived the manuscript. JPR conducted the literature review and wrote the manuscript, with feedback from AH, FF, JW, NSS, STH, CB, SL, and AE. The final version of this manuscript was reviewed and approved by all authors.

Competing interests

The authors declare no competing interests.

References

1. Ostrom, Q. T. *et al.* CBTRUS Statistical Report: Primary Brain and Other Central Nervous System Tumors Diagnosed in the United States in 2016—2020. *Neuro-Oncol.* **25**, iv1–iv99 (2023).
2. Weller, M. *et al.* Glioma. *Nat. Rev. Dis. Primer* **1**, 15017 (2015).
3. Yang, K. *et al.* Glioma targeted therapy: insight into future of molecular approaches. *Mol. Cancer* **21**, 39 (2022).
4. Stupp, R. *et al.* Radiotherapy plus Concomitant and Adjuvant Temozolomide for Glioblastoma. *N. Engl. J. Med.* **352**, 987–996 (2005).
5. Hegi, M. E. *et al.* MGMT Gene Silencing and Benefit from Temozolomide in Glioblastoma. *N. Engl. J. Med.* **352**, 997–1003 (2005).
6. Louis, D. N. *et al.* The 2021 WHO Classification of Tumors of the Central Nervous System: a summary. *Neuro-Oncol.* **23**, 1231–1251 (2021).
7. Horbinski, C., Berger, T., Packer, R. J. & Wen, P. Y. Clinical implications of the 2021 edition of the WHO classification of central nervous system tumours. *Nat. Rev. Neurol.* **18**, 515–529 (2022).
8. Echle, A. *et al.* Deep learning in cancer pathology: a new generation of clinical biomarkers. *Br. J. Cancer* **124**, 686–696 (2021).
9. Shmatko, A., Ghaffari Laleh, N., Gerstung, M. & Kather, J. N. Artificial intelligence in histopathology: enhancing cancer research and clinical oncology. *Nat. Cancer* **3**, 1026–1038 (2022).
10. Luo, J., Pan, M., Mo, K., Mao, Y. & Zou, D. Emerging role of artificial intelligence in diagnosis, classification and clinical management of glioma. *Semin. Cancer Biol.* **91**, 110–123 (2023).
11. Zadeh Shirazi, A. *et al.* The Application of Deep Convolutional Neural Networks to Brain Cancer Images: A Survey. *J. Pers. Med.* **10**, 224 (2020).
12. Sotoudeh, H. *et al.* Artificial Intelligence in the Management of Glioma: Era of

- Personalized Medicine. *Front. Oncol.* **9**, (2019).
13. Philip, A. K., Samuel, B. A., Bhatia, S., Khalifa, S. A. M. & El-Seedi, H. R. Artificial Intelligence and Precision Medicine: A New Frontier for the Treatment of Brain Tumors. *Life* **13**, 24 (2023).
 14. Bhatele, K. R. & Bhadauria, S. S. Machine learning application in Glioma classification: review and comparison analysis. *Arch. Comput. Methods Eng.* **29**, 247–274 (2022).
 15. Muhammad, K., Khan, S., Ser, J. D. & Albuquerque, V. H. C. de. Deep Learning for Multigrade Brain Tumor Classification in Smart Healthcare Systems: A Prospective Survey. *IEEE Trans. Neural Netw. Learn. Syst.* **32**, 507–522 (2021).
 16. Zhao, R. & Krauze, A. Survival Prediction in Gliomas: Current State and Novel Approaches. *Exon Publ.* 151–169 (2021)
doi:10.36255/exonpublications.gliomas.2021.chapter9.
 17. Alleman, K. *et al.* Multimodal Deep Learning-Based Prognostication in Glioma Patients: A Systematic Review. *Cancers* **15**, 545 (2023).
 18. Wijethilake, N. *et al.* Glioma Survival Analysis Empowered With Data Engineering—A Survey. *IEEE Access* **9**, 43168–43191 (2021).
 19. Zhang, P. *et al.* Effective nuclei segmentation with sparse shape prior and dynamic occlusion constraint for glioblastoma pathology images. *J. Med. Imaging* **6**, 017502 (2019).
 20. Liu, X.-P. *et al.* Clinical significance and molecular annotation of cellular morphometric subtypes in lower-grade gliomas discovered by machine learning. *Neuro-Oncol.* **25**, 68–81 (2023).
 21. Zadeh Shirazi, A. *et al.* A deep convolutional neural network for segmentation of whole-slide pathology images identifies novel tumour cell-perivascular niche interactions that are associated with poor survival in glioblastoma. *Br. J. Cancer* **125**, 337–350 (2021).
 22. Kalra, S. *et al.* Pan-cancer diagnostic consensus through searching archival histopathology images using artificial intelligence. *Npj Digit. Med.* **3**, 1–15 (2020).
 23. Faust, K. *et al.* Integrating morphologic and molecular histopathological features through

- whole slide image registration and deep learning. *Neuro-Oncol. Adv.* **4**, vdac001 (2022).
24. McLendon, R. *et al.* Comprehensive genomic characterization defines human glioblastoma genes and core pathways. *Nature* **455**, 1061–1068 (2008).
 25. Brennan, C. W. *et al.* The Somatic Genomic Landscape of Glioblastoma. *Cell* **155**, 462–477 (2013).
 26. The Cancer Genome Atlas Research Network. Comprehensive, Integrative Genomic Analysis of Diffuse Lower-Grade Gliomas. *N. Engl. J. Med.* **372**, 2481–2498 (2015).
 27. Jin, L. *et al.* Artificial intelligence neuropathologist for glioma classification using deep learning on hematoxylin and eosin stained slide images and molecular markers. *Neuro-Oncol.* **23**, 44–52 (2021).
 28. Im, S. *et al.* Classification of Diffuse Glioma Subtype from Clinical-Grade Pathological Images Using Deep Transfer Learning. *Sensors* **21**, 3500 (2021).
 29. Li, Z. *et al.* Vision transformer-based weakly supervised histopathological image analysis of primary brain tumors. *iScience* **26**, 105872 (2023).
 30. Shi, L. *et al.* Contribution of whole slide imaging-based deep learning in the assessment of intraoperative and postoperative sections in neuropathology. *Brain Pathol.* **33**, e13160 (2023).
 31. Xing, X. *et al.* A Multi-scale Graph Network with Multi-head Attention for Histopathology Image Diagnosis. in *Proceedings of the MICCAI Workshop on Computational Pathology* 227–235 (PMLR, 2021).
 32. Wang, X. *et al.* Machine Learning Models for Multiparametric Glioma Grading With Quantitative Result Interpretations. *Front. Neurosci.* **12**, (2019).
 33. Wang, X., Price, S. & Li, C. Multi-task Learning of Histology and Molecular Markers for Classifying Diffuse Glioma. in *Medical Image Computing and Computer Assisted Intervention – MICCAI 2023* (eds. Greenspan, H. *et al.*) 551–561 (Springer Nature Switzerland, Cham, 2023). doi:10.1007/978-3-031-43990-2_52.
 34. Hou, L. *et al.* Patch-Based Convolutional Neural Network for Whole Slide Tissue Image Classification. in *2016 IEEE Conference on Computer Vision and Pattern Recognition*

- (CVPR) 2424–2433 (2016). doi:10.1109/CVPR.2016.266.
35. Jose, L. *et al.* Artificial Intelligence–Assisted Classification of Gliomas Using Whole Slide Images. *Arch. Pathol. Lab. Med.* **147**, 916–924 (2022).
 36. Wang, X. *et al.* Combining Radiology and Pathology for Automatic Glioma Classification. *Front. Bioeng. Biotechnol.* **10**, (2022).
 37. Kurc, T. *et al.* Segmentation and Classification in Digital Pathology for Glioma Research: Challenges and Deep Learning Approaches. *Front. Neurosci.* **14**, (2020).
 38. Hsu, W.-W. *et al.* A weakly supervised deep learning-based method for glioma subtype classification using WSI and mpMRIs. *Sci. Rep.* **12**, 6111 (2022).
 39. Mousavi, H. S., Monga, V., Rao, G. & Rao, A. U. K. Automated discrimination of lower and higher grade gliomas based on histopathological image analysis. *J. Pathol. Inform.* **6**, 15 (2015).
 40. Mohan, G. & M, M. S. Intelligent framework for brain tumor grading using advanced feature analysis. *Comput. Methods Biomech. Biomed. Eng. Imaging Vis.* **11**, 485–503 (2023).
 41. Rathore, S., Niazi, T., Iftikhar, M. A. & Chaddad, A. Glioma Grading via Analysis of Digital Pathology Images Using Machine Learning. *Cancers* **12**, 578 (2020).
 42. Barker, J., Hoogi, A., Depeursinge, A. & Rubin, D. L. Automated classification of brain tumor type in whole-slide digital pathology images using local representative tiles. *Med. Image Anal.* **30**, 60–71 (2016).
 43. Fukuma, K., Surya Prasath, V. B., Kawanaka, H., Aronow, B. J. & Takase, H. A study on feature extraction and disease stage classification for Glioma pathology images. in *2016 IEEE International Conference on Fuzzy Systems (FUZZ-IEEE)* 2150–2156 (2016). doi:10.1109/FUZZ-IEEE.2016.7737958.
 44. Reza, S. M. S. & Iftikharuddin, K. M. Glioma grading using cell nuclei morphologic features in digital pathology images. in *Medical Imaging 2016: Computer-Aided Diagnosis* vol. 9785 735–740 (SPIE, 2016).
 45. Pei, L., Jones, K. A., Shboul, Z. A., Chen, J. Y. & Iftikharuddin, K. M. Deep Neural

- Network Analysis of Pathology Images With Integrated Molecular Data for Enhanced Glioma Classification and Grading. *Front. Oncol.* **11**, (2021).
46. Truong, A. H., Sharmanska, V., Limbäck-Stanic, C. & Grech-Sollars, M. Optimization of deep learning methods for visualization of tumor heterogeneity and brain tumor grading through digital pathology. *Neuro-Oncol. Adv.* **2**, (2020).
47. Ertosun, M. G. & Rubin, D. L. Automated Grading of Gliomas using Deep Learning in Digital Pathology Images: A modular approach with ensemble of convolutional neural networks. *AMIA. Annu. Symp. Proc.* **2015**, 1899–1908 (2015).
48. Su, F. *et al.* Annotation-free glioma grading from pathological images using ensemble deep learning. *Heliyon* **9**, e14654 (2023).
49. Momeni, A., Thibault, M. & Gevaert, O. Deep Recurrent Attention Models for Histopathological Image Analysis. 438341 Preprint at <https://doi.org/10.1101/438341> (2018).
50. Qiu, L. *et al.* Hierarchical multimodal fusion framework based on noisy label learning and attention mechanism for cancer classification with pathology and genomic features. *Comput. Med. Imaging Graph.* **104**, 102176 (2023).
51. Chen, R. J. *et al.* Pathomic Fusion: An Integrated Framework for Fusing Histopathology and Genomic Features for Cancer Diagnosis and Prognosis. *IEEE Trans. Med. Imaging* **41**, 757–770 (2022).
52. Xing, X. *et al.* Discrepancy and Gradient-Guided Multi-modal Knowledge Distillation for Pathological Glioma Grading. in *Medical Image Computing and Computer Assisted Intervention – MICCAI 2022* (eds. Wang, L., Dou, Q., Fletcher, P. T., Speidel, S. & Li, S.) 636–646 (Springer Nature Switzerland, Cham, 2022).
doi:10.1007/978-3-031-16443-9_61.
53. Saldanha, O. L. *et al.* Self-supervised attention-based deep learning for pan-cancer mutation prediction from histopathology. *Npj Precis. Oncol.* **7**, 1–5 (2023).
54. Arslan, S. *et al.* Deep learning can predict multi-omic biomarkers from routine pathology images: A systematic large-scale study. 2022.01.21.477189 Preprint at

<https://doi.org/10.1101/2022.01.21.477189> (2022).

55. Loeffler, C. M. L. *et al.* Predicting Mutational Status of Driver and Suppressor Genes Directly from Histopathology With Deep Learning: A Systematic Study Across 23 Solid Tumor Types. *Front. Genet.* **12**, (2022).
56. Liu, S. *et al.* Isocitrate dehydrogenase (IDH) status prediction in histopathology images of gliomas using deep learning. *Sci. Rep.* **10**, 7733 (2020).
57. Wang, D. *et al.* Automated Machine-Learning Framework Integrating Histopathological and Radiological Information for Predicting IDH1 Mutation Status in Glioma. *Front. Bioinforma.* **1**, (2021).
58. Jiang, S., Zanazzi, G. J. & Hassanpour, S. Predicting prognosis and IDH mutation status for patients with lower-grade gliomas using whole slide images. *Sci. Rep.* **11**, 16849 (2021).
59. Liechty, B. *et al.* Machine learning can aid in prediction of IDH mutation from H&E-stained histology slides in infiltrating gliomas. *Sci. Rep.* **12**, 22623 (2022).
60. Gorlia, T. *et al.* Nomograms for predicting survival of patients with newly diagnosed glioblastoma: prognostic factor analysis of EORTC and NCIC trial 26981-22981/CE.3. *Lancet Oncol.* **9**, 29–38 (2008).
61. Nalisnik, M. *et al.* Interactive phenotyping of large-scale histology imaging data with HistomicsML. *Sci. Rep.* **7**, 14588 (2017).
62. Luo, C., Yang, J., Liu, Z. & Jing, D. Predicting the recurrence and overall survival of patients with glioma based on histopathological images using deep learning. *Front. Neurol.* **14**, (2023).
63. Baheti, B. *et al.* Detecting Histologic & Clinical Glioblastoma Patterns of Prognostic Relevance. Preprint at <https://doi.org/10.48550/arXiv.2302.00669> (2023).
64. Zhang, Y., Li, A., He, J. & Wang, M. A Novel MKL Method for GBM Prognosis Prediction by Integrating Histopathological Image and Multi-Omics Data. *IEEE J. Biomed. Health Inform.* **24**, 171–179 (2020).
65. Powell, R. T. *et al.* Identification of Histological Correlates of Overall Survival in Lower

- Grade Gliomas Using a Bag-of-words Paradigm: A Preliminary Analysis Based on Hematoxylin & Eosin Stained Slides from the Lower Grade Glioma Cohort of The Cancer Genome Atlas. *J. Pathol. Inform.* **8**, 9 (2017).
66. Zadeh Shirazi, A. *et al.* DeepSurvNet: deep survival convolutional network for brain cancer survival rate classification based on histopathological images. *Med. Biol. Eng. Comput.* **58**, 1031–1045 (2020).
67. Liu, P., Fu, B., Ye, F., Yang, R. & Ji, L. DSCA: A dual-stream network with cross-attention on whole-slide image pyramids for cancer prognosis. *Expert Syst. Appl.* **227**, 120280 (2023).
68. Wang, Z. *et al.* Surformer: An interpretable pattern-perceptive survival transformer for cancer survival prediction from histopathology whole slide images. *Comput. Methods Programs Biomed.* **241**, 107733 (2023).
69. Chen, R. J. *et al.* Multimodal Co-Attention Transformer for Survival Prediction in Gigapixel Whole Slide Images. in 4015–4025 (2021).
70. Zhu, X., Yao, J., Zhu, F. & Huang, J. WSISA: Making Survival Prediction from Whole Slide Histopathological Images. in *2017 IEEE Conference on Computer Vision and Pattern Recognition (CVPR)* 6855–6863 (2017). doi:10.1109/CVPR.2017.725.
71. Klemm, F. *et al.* Interrogation of the Microenvironmental Landscape in Brain Tumors Reveals Disease-Specific Alterations of Immune Cells. *Cell* **181**, 1643-1660.e17 (2020).
72. Cordell, E. C., Alghamri, M. S., Castro, M. G. & Gutmann, D. H. T lymphocytes as dynamic regulators of glioma pathobiology. *Neuro-Oncol.* **24**, 1647–1657 (2022).
73. Zhu, X., Yao, J. & Huang, J. Deep convolutional neural network for survival analysis with pathological images. in *2016 IEEE International Conference on Bioinformatics and Biomedicine (BIBM)* 544–547 (2016). doi:10.1109/BIBM.2016.7822579.
74. Li, R., Yao, J., Zhu, X., Li, Y. & Huang, J. Graph CNN for Survival Analysis on Whole Slide Pathological Images. in *Medical Image Computing and Computer Assisted Intervention – MICCAI 2018* (eds. Frangi, A. F., Schnabel, J. A., Davatzikos, C., Alberola-López, C. & Fichtinger, G.) 174–182 (Springer International Publishing, Cham,

2018). doi:10.1007/978-3-030-00934-2_20.

75. Chen, R. J. *et al.* Whole Slide Images are 2D Point Clouds: Context-Aware Survival Prediction Using Patch-Based Graph Convolutional Networks. in *Medical Image Computing and Computer Assisted Intervention – MICCAI 2021* (eds. de Bruijne, M. *et al.*) 339–349 (Springer International Publishing, Cham, 2021).
doi:10.1007/978-3-030-87237-3_33.
76. Jiang, S., Suriawinata, A. A. & Hassanpour, S. MHAttnSurv: Multi-head attention for survival prediction using whole-slide pathology images. *Comput. Biol. Med.* **158**, 106883 (2023).
77. Carmichael, I. *et al.* Incorporating Intratumoral Heterogeneity into Weakly-Supervised Deep Learning Models via Variance Pooling. in *Medical Image Computing and Computer Assisted Intervention – MICCAI 2022* (eds. Wang, L., Dou, Q., Fletcher, P. T., Speidel, S. & Li, S.) 387–397 (Springer Nature Switzerland, Cham, 2022).
doi:10.1007/978-3-031-16434-7_38.
78. Chunduru, P., Phillips, J. J. & Molinaro, A. M. Prognostic risk stratification of gliomas using deep learning in digital pathology images. *Neuro-Oncol. Adv.* **4**, vdac111 (2022).
79. Mobadersany, P. *et al.* Predicting cancer outcomes from histology and genomics using convolutional networks. *Proc. Natl. Acad. Sci.* **115**, E2970–E2979 (2018).
80. Chen, R. J. *et al.* Pan-cancer integrative histology-genomic analysis via multimodal deep learning. *Cancer Cell* **40**, 865-878.e6 (2022).
81. Braman, N. *et al.* Deep Orthogonal Fusion: Multimodal Prognostic Biomarker Discovery Integrating Radiology, Pathology, Genomic, and Clinical Data. Preprint at <https://doi.org/10.48550/arXiv.2107.00648> (2021).
82. Xu, Y. *et al.* Large scale tissue histopathology image classification, segmentation, and visualization via deep convolutional activation features. *BMC Bioinformatics* **18**, 281 (2017).
83. Krebs, O., Agarwal, S. & Tiwari, P. Self-supervised deep learning to predict molecular markers from routine histopathology slides for high-grade glioma tumors. in *Medical*

- Imaging 2023: Digital and Computational Pathology* vol. 12471 1247102 (SPIE, 2023).
84. He, K., Zhang, X., Ren, S. & Sun, J. Deep Residual Learning for Image Recognition. Preprint at <https://doi.org/10.48550/arXiv.1512.03385> (2015).
 85. Simonyan, K. & Zisserman, A. Very Deep Convolutional Networks for Large-Scale Image Recognition. Preprint at <https://doi.org/10.48550/arXiv.1409.1556> (2015).
 86. Huang, G., Liu, Z., van der Maaten, L. & Weinberger, K. Q. Densely Connected Convolutional Networks. Preprint at <https://doi.org/10.48550/arXiv.1608.06993> (2018).
 87. Tan, M. & Le, Q. V. EfficientNet: Rethinking Model Scaling for Convolutional Neural Networks. Preprint at <https://doi.org/10.48550/arXiv.1905.11946> (2020).
 88. Szegedy, C. *et al.* Going Deeper with Convolutions. Preprint at <https://doi.org/10.48550/arXiv.1409.4842> (2014).
 89. Krizhevsky, A., Sutskever, I. & Hinton, G. E. ImageNet Classification with Deep Convolutional Neural Networks. in *Advances in Neural Information Processing Systems* vol. 25 (Curran Associates, Inc., 2012).
 90. Yang, P. *et al.* CS-CO: A Hybrid Self-Supervised Visual Representation Learning Method for H&E-stained Histopathological Images. *Med. Image Anal.* **81**, 102539 (2022).
 91. Lu, M. *et al.* SMILE: Sparse-Attention based Multiple Instance Contrastive Learning for Glioma Sub-Type Classification Using Pathological Images. in *Proceedings of the MICCAI Workshop on Computational Pathology* 159–169 (PMLR, 2021).
 92. Zhang, L. *et al.* Mutual Contrastive Low-rank Learning to Disentangle Whole Slide Image Representations for Glioma Grading. Preprint at <https://doi.org/10.48550/arXiv.2203.04013> (2022).
 93. Cheerla, A. & Gevaert, O. Deep learning with multimodal representation for pancancer prognosis prediction. *Bioinformatics* **35**, i446–i454 (2019).
 94. Jiang, S., Hondelink, L., Suriawinata, A. A. & Hassanpour, S. Masked Pre-Training of Transformers for Histology Image Analysis. Preprint at <https://doi.org/10.48550/arXiv.2304.07434> (2023).
 95. Chitnis, S. R. *et al.* Domain-Specific Pre-training Improves Confidence in Whole Slide

- Image Classification. Preprint at <https://doi.org/10.48550/arXiv.2302.09833> (2023).
96. Suman, S. & Prasanna, P. Multi-stage attention-based network for brain tumor subtype classification. in *Medical Imaging 2022: Digital and Computational Pathology* vol. 12039 272–276 (SPIE, 2022).
97. Kleppe, A. *et al.* Designing deep learning studies in cancer diagnostics. *Nat. Rev. Cancer* **21**, 199–211 (2021).
98. Howard, F. M. *et al.* The impact of site-specific digital histology signatures on deep learning model accuracy and bias. *Nat. Commun.* **12**, 4423 (2021).
99. Howard, F. M., Kather, J. N. & Pearson, A. T. Multimodal deep learning: An improvement in prognostication or a reflection of batch effect? *Cancer Cell* **41**, 5–6 (2023).
100. Homeyer, A. *et al.* Recommendations on compiling test datasets for evaluating artificial intelligence solutions in pathology. *Mod. Pathol.* **35**, 1759–1769 (2022).
101. Brindha, V., Jayashree, P., Karthik, P. & Manikandan, P. Tumor grading model employing geometric analysis of histopathological images with characteristic nuclei dictionary. *Comput. Biol. Med.* **149**, 106008 (2022).
102. Yonekura, A., Kawanaka, H., Prasath, V. B. S., Aronow, B. J. & Takase, H. Automatic disease stage classification of glioblastoma multiforme histopathological images using deep convolutional neural network. *Biomed. Eng. Lett.* **8**, 321–327 (2018).
103. Hao, J., Kosaraju, S. C., Tsaku, N. Z., Song, D. H. & Kang, M. PAGE-Net: Interpretable and Integrative Deep Learning for Survival Analysis Using Histopathological Images and Genomic Data. in *Biocomputing 2020* 355–366 (WORLD SCIENTIFIC, 2019).
doi:10.1142/9789811215636_0032.
104. Chen, L. *et al.* Predicting the likelihood of an isocitrate dehydrogenase 1 or 2 mutation in diagnoses of infiltrative glioma. *Neuro-Oncol.* **16**, 1478–1483 (2014).
105. Ghaffari Laleh, N. *et al.* Benchmarking weakly-supervised deep learning pipelines for whole slide classification in computational pathology. *Med. Image Anal.* **79**, 102474 (2022).
106. Boehm, K. M., Khosravi, P., Vanguri, R., Gao, J. & Shah, S. P. Harnessing multimodal

- data integration to advance precision oncology. *Nat. Rev. Cancer* **22**, 114–126 (2022).
107. Ker, J., Bai, Y., Lee, H. Y., Rao, J. & Wang, L. Automated brain histology classification using machine learning. *J. Clin. Neurosci.* **66**, 239–245 (2019).
108. Rathore, S., Iftikhar, M. A. & Mourelatos, Z. Prediction of overall survival and molecular markers in gliomas via analysis of digital pathology images using deep learning. Preprint at <https://doi.org/10.48550/arXiv.1909.09124> (2019).
109. Zheng, H., Momeni, A., Cedoz, P.-L., Vogel, H. & Gevaert, O. Whole slide images reflect DNA methylation patterns of human tumors. *Npj Genomic Med.* **5**, 1–10 (2020).
110. Tang, B., Li, A., Li, B. & Wang, M. CapSurv: Capsule Network for Survival Analysis With Whole Slide Pathological Images. *IEEE Access* **7**, 26022–26030 (2019).
111. Liu, P., Ji, L., Ye, F. & Fu, B. AdvMIL: Adversarial multiple instance learning for the survival analysis on whole-slide images. *Med. Image Anal.* **91**, 103020 (2024).

Figures

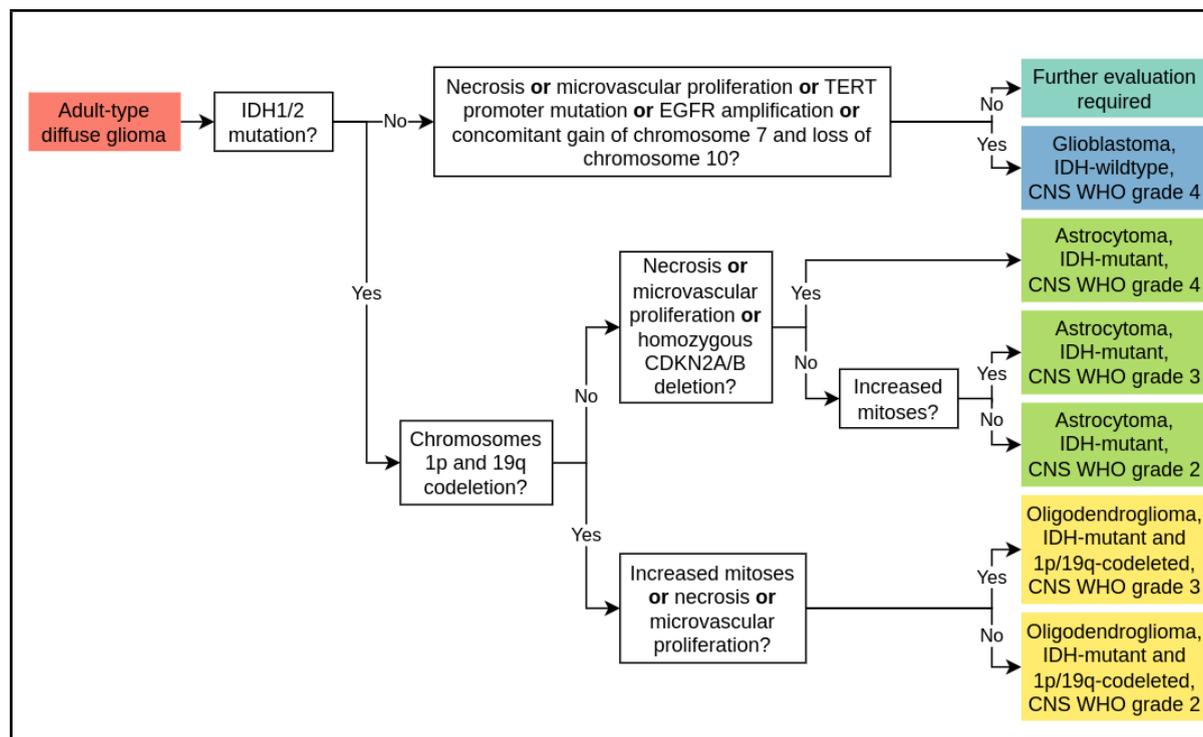


Figure 1: Schematic diagnostic algorithm for adult-type diffuse glioma as defined by the 2021 WHO Classification of Tumors of the Central Nervous System. The 2021 WHO classification system reorganizes gliomas into adult-type diffuse gliomas, pediatric-type diffuse low-grade and high-grade gliomas, circumscribed astrocytic gliomas, and ependymal tumors⁶. Adult-type diffuse gliomas comprise Glioblastoma, IDH-wildtype, CNS WHO grade 4, Astrocytoma, IDH-mutant, CNS WHO grade 2–4 and Oligodendroglioma, IDH-mutant and 1p/19q-codeleted, CNS WHO grade 2–3⁶. Identified adult-type diffuse glioma are stratified from left to right according to molecular alterations, including mutations in isocitrate dehydrogenase 1/2 (IDH1/2) genes and whole-arm codeletion of chromosomes 1p and 19q, as well as histological features, including increased mitoses, necrosis and/or microvascular proliferation. “or” is understood to be non-exclusive. Figure inspired by Horbinski et al. (2022)⁷.

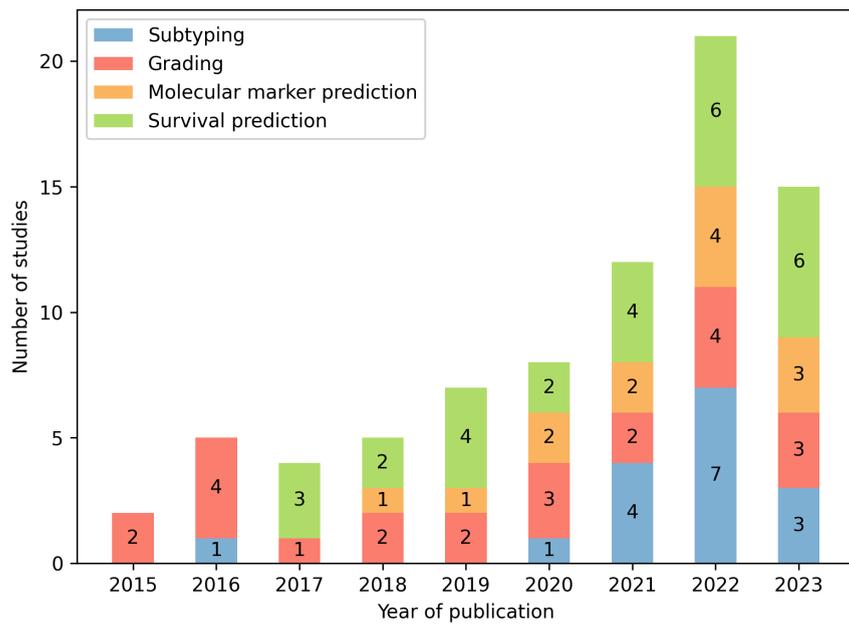


Figure 2: Number of studies by year of publication and diagnostic task. All 70 studies included in this review are shown. Studies published in 2023 are considered up until June 2, 2023.

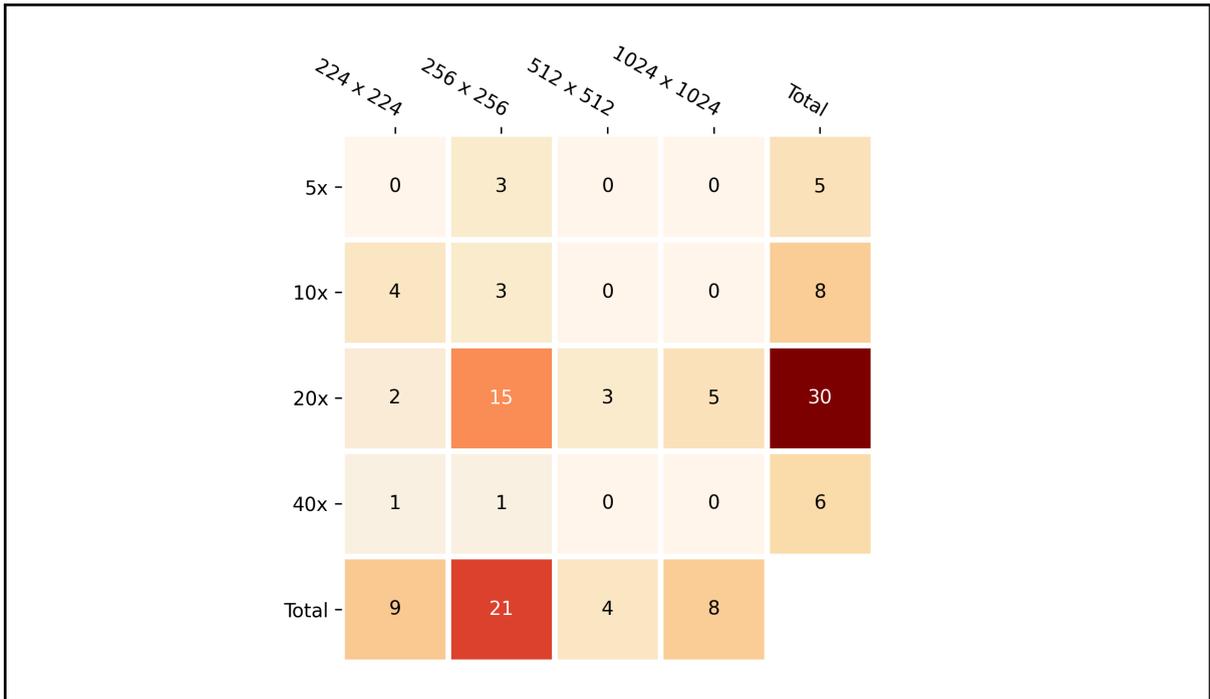


Figure 3: Patch sizes and magnifications employed by studies. Studies were taken into account if at least one of the two pieces of information was specified. Other patch sizes and magnifications employed by single studies (e.g. 150 x 150 pixels, 4x magnification) are not shown.

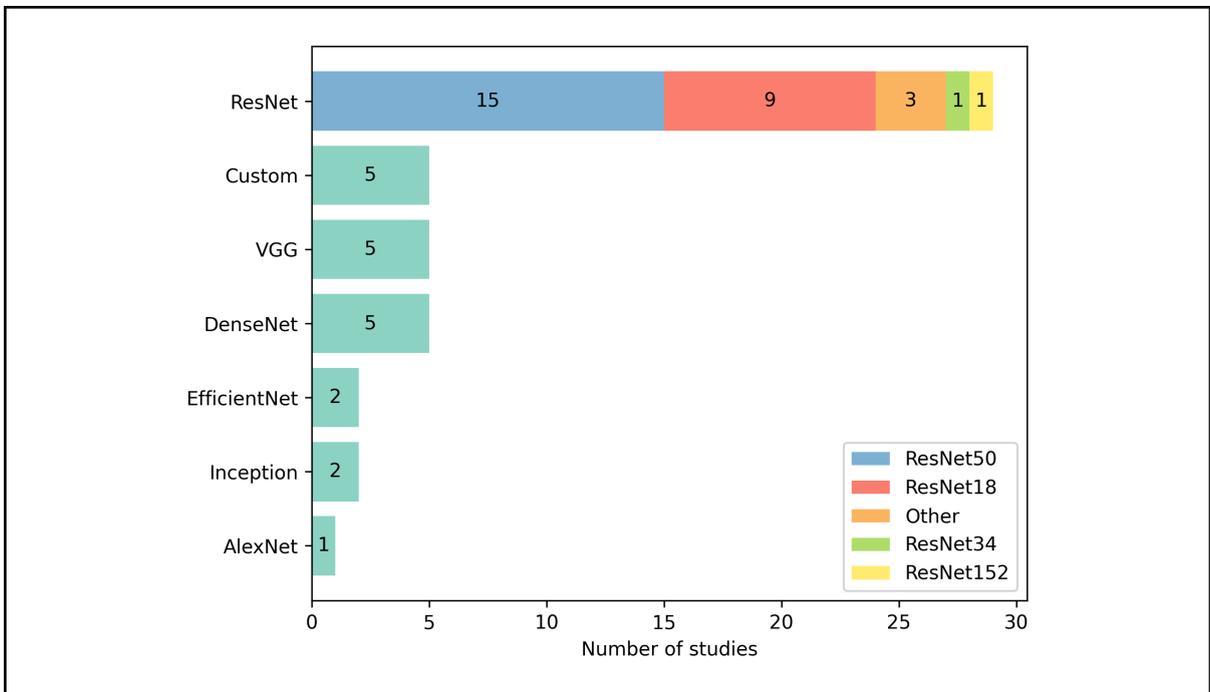


Figure 4: Convolutional neural network architectures employed by studies. With only a few exceptions all convolutional neural networks were pre-trained using the ImageNet dataset. Except for ResNet architectures exact variants of stated architectures are not shown. “Custom” refers to custom, i.e. self-configured architectures.

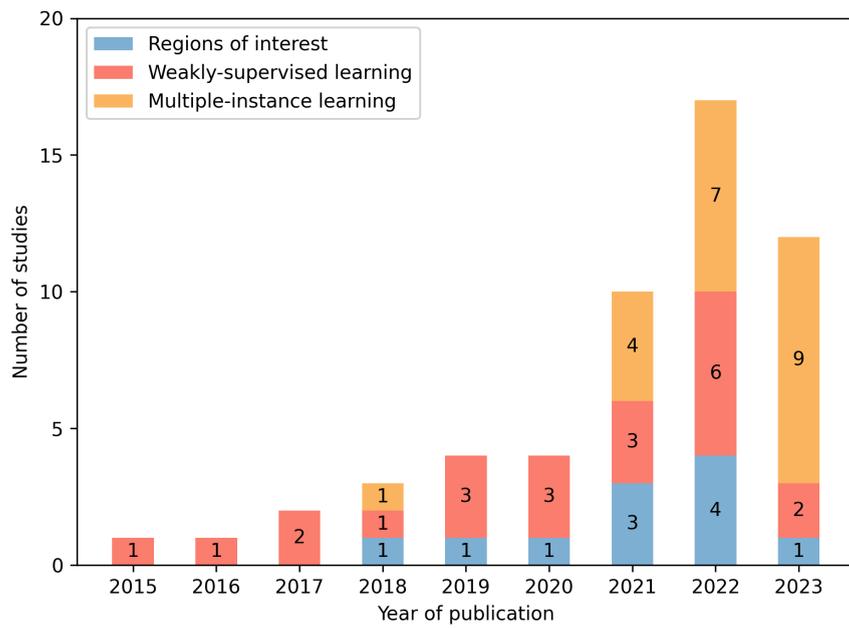


Figure 5: Learning paradigms employed by studies. Usage of regions of interest, weakly-supervised learning and multiple-instance learning by all 57 deep learning-based studies included in this review distributed by year of publication. Methodological differences of the three approaches are explained in Box 1.

Whole-slide images (WSIs)	WSIs are digitized microscopic images of whole tissue sections. As they are scanned with a very high resolution of up to 0.25 micrometers per pixel, WSIs can be several gigapixels in size. To enable faster access, WSIs are usually stored as image pyramids consisting of several magnification levels, which are labeled according to the comparable objective magnifications of an analogue microscope (e.g., 5x, 10x, 20x, or 40x). The large size and the great variability and complexity of depicted morphological patterns makes analysis of WSI very challenging.
Regions of interest (ROIs)	As tumor tissue sections naturally include different tissue types, some AI models require a delineation of ROIs of relevant tumor tissue. Usually, this delineation is a laborious task which requires expert knowledge.
Patch-based processing of WSIs	Due to their gigapixel size, WSIs and ROIs are usually processed by partitioning them into smaller image patches (or tiles) and processing patches individually. This greatly reduces the memory requirements and facilitates parallelization.
Weakly-supervised learning (WSL)	In WSL, each patch inherits the reference label of the entire WSI irrespective of the actual patch content ¹⁰⁵ . The patch-level information is subsequently aggregated to infer a WSI-level prediction. WSL avoids the effort of annotating ROIs, but the resulting label noise can reduce predictive performance.
Multiple-instance learning (MIL)	MIL also works without ROI annotations but addresses the conceptual limitations of WSL. Concrete implementations of MIL often feature intricate architectures to model complex interactions among patches ¹⁰⁵ .
Multi-modal fusion	Fusing WSIs with other modalities of potentially complementary information, such as MRI, clinical, or omics data, poses great opportunities for improving diagnostic and prognostic precision ¹⁰⁶ . Common approaches can be differentiated by the extent to which given modalities are processed in combination before predictions are inferred: Early fusion concatenates modalities at the onset; late fusion aggregates individual uni-modal predictions, e.g. by averaging; and intermediate fusion infers final predictions from an intermediate multi-modal representation ¹⁰⁶ .
Box 1: Key concepts of artificial intelligence-based analysis of WSIs.	

Tables

Study	Method		Multi-modal fusion		Dataset					Performance	
	Features	Learning paradigm	Modalities	Fusion Strategy	TCGA-GBM	TCGA-LGG	Other	#Patients	#WSIs	Metric	Result
Astrocytoma vs. Oligodendroglioma vs. Glioblastoma											
Wang et al. (2023) ³³	ViT	MIL	H&E		X	X		940	2633	ACC	0.773
Hsu et al. (2022) ³⁸	CNN (ResNet50)	WSL	H&E, MRI	Late	X	X	X	329		balanced ACC	0.654
Jose et al. (2022) ³⁵	CNN (ResNet50)	WSL	H&E		X	X		700	926	AUC	0.961
Suman et al. (2022) ⁹⁶	CNN	WSL, MIL	H&E		X	X		230		balanced ACC	0.730
Wang et al. (2022) ³⁶	CNN (EfficientNet-B2, EfficientNet-B3, SEResNeXt101)	WSL	H&E, MRI, clinical	Late	X	X	X	378		balanced ACC	0.889
Lu et al. (2021) ⁹¹	CNN (ResNet50)	SSL, MIL	H&E	Intermediate	X	X		700	700	ACC	0.886
Astrocytoma vs. Anaplastic Astrocytoma vs. Oligodendroglioma vs. Anaplastic Oligodendroglioma vs. Glioblastoma											
Li et al. (2023) ²⁹	ViT (ViT-L-16)	MIL	H&E		X	X	X	749, 597 ^a	1487, 2754 ^a	AUC	0.932, 0.880 ^a
Jin et al. (2021) ²⁷	CNN (DenseNet)	WSL	H&E				X	323	323	ACC	0.865
Xing et al. (2021) ³¹	CNN (DenseNet)	WSL	H&E				X		440	ACC	0.700
Astrocytoma vs. Anaplastic Astrocytoma vs. Oligodendroglioma vs. Anaplastic Oligodendroglioma vs. Oligoastrocytoma vs. Glioblastoma											
Hou et al. (2016) ³⁴	CNN	WSL	H&E		X	X		539	1064	ACC	0.771
Astrocytoma IDH-mutant vs. Astrocytoma IDH-wildtype vs. Oligodendroglioma IDH-mutant 1p/19q codeleted											
Faust et al. (2022) ²³	CNN (VGG19)	SL	H&E, IHC	Late			X		1013	ACC	1.0

Astrocytoma IDH-mutant vs. Astrocytoma IDH-wildtype vs. Oligodendroglioma IDH-wildtype vs. Glioblastoma IDH-mutant vs. Glioblastoma IDH-wildtype											
Chitnis et al. (2023) ⁹⁵	CNN (KimiaNet)	MIL	H&E				X	791	866	AUC	0.969
Oligodendroglioma vs. Non-Oligodendroglioma											
Im et al. (2021) ²⁸	CNN (ResNet50)	ROIs	H&E				X	369		balanced ACC	0.873
Astrocytoma vs. Oligodendroglioma											
Kurc et al. (2020) ³⁷	CNN (DenseNet)	WSL	H&E, MRI	Late		X		52		ACC	0.900
Astrocytoma vs. Oligodendroglioma vs. Intracranial Germinoma											
Shi et al. (2023) ³⁰	CNN (ResNet152)	WSL	H&E, IFS			X	X	346	832	ACC	0.769, 0.820 ^b
Astrocytic vs. Oligodendroglial vs. Ependymal											
Yang et al. (2022) ⁹⁰	CNN (ResNet18)	SSL, MIL	H&E				X		935	weighted F1-score	0.780
<p>Table 1: Overview of all studies related to subtyping. Studies are organized into specific subtasks and sorted by year of publication. Columns “TCGA-GBM”, “TCGA-LGG” and “Other” indicate whether TCGA-GBM, TCGA-LGG and/or other public or proprietary datasets were employed. “#Patients” and “#WSIs” state the reported size of the dataset including subsets for training and validation. “Performance” states a selection of the reported performance metrics. CNN = convolutional neural network, ViT = Vision Transformer, ROI = region of interest, SL = supervised learning, WSL = weakly-supervised learning, SSL = self-supervised learning, MIL = multiple-instance learning, H&E = hematoxylin and eosin staining, MRI = magnetic resonance imaging, IHC = immunohistochemistry, IFS = intraoperative frozen sections, ACC = accuracy, AUC = area under the operator receiver curve, ^a = for A vs. AA vs. O vs. AO vs. GBM vs. six meningioma types, ^b = for model based on intraoperative frozen sections.</p>											

Study	Method		Multi-modal fusion		Dataset					Performance	
	Features	Learning paradigm	Modalities	Fusion Strategy	TCGA-GBM	TCGA-LGG	Other	#Patients	#WSIs	Metric	Result
WHO grade II vs. WHO grade III vs. WHO grade IV											
Qiu et al. (2023) ⁵⁰	CNN (ResNet)	ROIs	H&E, omics	Intermediate	X	X		683	683	AUC	0.872
Zhang et al. (2022) ⁹²	CNN (EfficientNet-B0)	SSL, MIL	H&E		X	X		499		ACC	0.790 ^a , 0.750 ^b
Xing et al. (2022) ⁵²	CNN (ResNet18)	ROIs	H&E, omics		X	X		736	1325*	AUC	0.924
Pei et al. (2021) ⁴⁵	CNN (ResNet)	WSL	H&E, omics	Early	X	X			549	ACC	0.938 ^c , 0.740 ^d
Chen et al. (2022) ⁵¹	CNN (VGG19)	ROIs	H&E, omics	Intermediate	X	X		769	1505*	AUC	0.908
Truong et al. (2020) ⁴⁶	CNN (ResNet18)	WSL	H&E		X	X		1120	3611	ACC	0.730 ^c , 0.530 ^d
Wang et al. (2019) ³²	Handcrafted		H&E, proliferation index	Early			X	146		ACC	0.900
Ertosun et al. (2015) ⁴⁷	CNN	WSL	H&E		X	X			37	ACC	0.960 ^c , 0.710 ^d
WHO grade II and III vs. WHO grade IV											
Jiang et al. (2023) ⁹⁴	CNN (ResNet18)	SSL, MIL	H&E		X	X				AUC	0.964
Brindha et al. (2022) ¹⁰¹	Handcrafted		H&E		X	X			1114	ACC	0.972
Mohan et al. (2022) ⁴⁰	Handcrafted		H&E		X	X			310	AUC	0.974
Im et al. (2021) ²⁸	CNN (MnasNet)	ROIs	H&E				X	468		balanced ACC	0.580
Rathore et al. (2020) ⁴¹	Handcrafted	ROIs	H&E, clinical	Early	X	X		735		AUC	0.927
Momeni et al. (2018) ⁴⁹	CNN	WSL	H&E		X	X		710		AUC	0.930
Yonekura et al. (2018) ¹⁰²	CNN	WSL	H&E		X	X			200	ACC	0.965

Xu et al. (2017) ⁸²	CNN (AlexNet)	WSL	H&E				X		85	ACC	0.975
Barker et al. (2016) ⁴²	Handcrafted		H&E		X	X	X		649	AUC	0.960
Hou et al. (2016) ³⁴	CNN	WSL	H&E		X	X		539	1064	ACC	0.970
Reza et al. (2016) ⁴⁴	Handcrafted		H&E		X	X			66	AUC	0.955
Fukuma et al. (2016) ⁴³	Handcrafted		H&E		X	X			300	ACC	0.996
WHO grade II vs. WHO grade III											
Su et al. (2023) ⁴⁸	CNN (ResNet18)	WSL	H&E			X		507		ACC	0.801
Non-tumor vs. WHO grade II and III vs. WHO grade IV											
Ker et al. (2019) ¹⁰⁷	CNN (InceptionV3)	WSL	H&E				X		154**	F1-score	0.991
WHO grade I and II vs. WHO grade III and IV											
Mousavi et al. (2015) ³⁹	Handcrafted		H&E		X	X		138		ACC	0.847
<p>Table 2: Overview of all studies related to grading. Studies are organized into specific subtasks and sorted by year of publication. Columns “TCGA-GBM”, “TCGA-LGG” and “Other” indicate whether TCGA-GBM, TCGA-LGG and/or other public or proprietary datasets were employed. “#Patients” and “#WSIs” state the reported size of the dataset including subsets for training and validation. “Performance” states a selection of the reported performance metrics. CNN = convolutional neural network, ROI = region of interest, SL = supervised learning, WSL = weakly-supervised learning, SSL = self-supervised learning, MIL = multiple-instance learning, H&E = hematoxylin and eosin staining, ACC = accuracy, AUC = area under the operator receiver curve, ^a = on frozen sections, ^b = on FFPE sections, ^c = for II+III vs. IV prediction, ^d = for II vs. III prediction, * = not WSIs but ROIs, ** = not gigapixel size WSIs but smaller images.</p>											

Study	Method		Multi-modal fusion		Dataset					Performance	
	Features	Learning paradigm	Modalities	Fusion Strategy	TCGA-GBM	TCGA-LGG	Other	#Patients	#WSIs	Metric	Result
IDH mutation											
Liechty et al. (2022) ⁵⁹	CNN (DenseNet121)	WSL	H&E		X	X	X	513	975	AUC	0.881
Jiang et al. (2021) ⁵⁸	CNN (ResNet18)	WSL	H&E, clinical	Early		X		490	843	AUC	0.814
Wang et al. (2021) ⁵⁷	Handcrafted		H&E, MRI	Late	X	X	X	217		ACC	0.900
Liu et al. (2020) ⁵⁶	CNN (ResNet50)	WSL	H&E, clinical	Early	X	X	X	266		AUC	0.931
IDH mutation, MGMT promoter methylation											
Krebs et al. (2023) ⁸³	CNN (ResNet18)	SSL, MIL	H&E		X			325	196 ^f , 216 ^g	ACC	0.912 ^a , 0.861 ^b
IDH mutation, MGMT promoter methylation, TP53 mutation											
Li et al. (2023) ²⁹	ViT (ViT-L-16)	MIL	H&E		X	X	X	1005 ^f , 257 ^g , 877 ^h		AUC	0.960 ^a , 0.845 ^b , 0.874 ^c
IDH mutation, MGMT promoter methylation, 1p/19q codeletion											
Momeni et al. (2018) ⁴⁹	CNN	WSL	H&E		X	X		710		AUC	0.860 ^f , 0.750 ^b , 0.760 ^d
IDH mutation, 1p/19q codeletion											
Rathore et al. (2019) ¹⁰⁸	CNN (ResNet)	ROIs	H&E		X	X		663		AUC	0.860 ^a , 0.860 ^d
IDH mutation, 1p/19q codeletion, homozygous deletion of CDKN2A/B											
Wang et al. (2023) ³³	ViT	MIL	H&E		X	X		940	2633	AUC	0.920 ^a , 0.881 ^d , 0.772 ^e
DNA methylation											
Zheng et al. (2020) ¹⁰⁹	Handcrafted		H&E, clinical	Early	X	X		327		AUC	0.740

Pan-cancer studies											
Saldanha et al. (2023) ⁵³	CNN (ResNet50)	SSL, MIL	H&E		X		X	493		AUC	0.840 ^a , 0.700 ^c , 0.700 ^f
Arslan et al. (2022) ⁵⁴	Autoencoder (ResNet34)	WSL	H&E		X	X	X	894	1999	AUC	0.669 ^g
Loeffler et al. (2022) ⁵⁵	CNN (ShuffleNet)	ROIs	H&E		X	X		680		AUC	0.764 ^a , 0.787 ^c , 0.726 ^f

Table 3: Overview of all studies related to molecular marker prediction. Studies are organized into specific subtasks and sorted by year of publication. Columns “TCGA-GBM”, “TCGA-LGG” and “Other” indicate whether TCGA-GBM, TCGA-LGG and/or other public or proprietary datasets were employed. “#Patients” and “#WSIs” state the reported size of the dataset including subsets for training and validation. “Performance” states a selection of the reported performance metrics. CNN = convolutional neural network, ViT = Vision Transformer, SL = supervised learning, ROI = region of interest, WSL = weakly-supervised learning, SSL = self-supervised learning, MIL = multiple-instance learning, H&E = hematoxylin and eosin staining, MRI = magnetic resonance imaging, ACC = accuracy, AUC = area under the operator receiver curve, ^a = for IDH mutation prediction, ^b = for MGMT promoter methylation prediction, ^c = for TP53 mutation prediction, ^d = for 1p/19q codeletion prediction, ^e = for CDKN2A/B prediction, ^f = for ATRX prediction, ^g = average performance across all predicted markers.

Study	Method		Multi-modal fusion		Dataset					Performance	
	Features	Learning paradigm	Modalities	Fusion Strategy	TCGA-GBM	TCGA-LGG	Other	#Patients	#WSIs	Metric	Result
Risk score / survival time regression											
Jiang et al. (2023) ⁷⁶	CNN (ResNet18)	MIL	H&E			X		490	843	C-index	0.714
Jiang et al. (2023) ⁹⁴	CNN (ResNet18)	SSL, MIL	H&E			X				C-index	0.685
Liu et al. (2023) ⁶⁷	CNN (ResNet50)	MIL	H&E			X		486	836	C-index	0.702
Luo et al. (2023) ⁶²	CNN (ResNet50)		H&E, clinical	Early			X	162		C-index	0.928**
Wang et al. (2023) ⁶⁸	CNN (ResNet50)	MIL	H&E		X	X		1041		C-index	0.861
Carmichael et al. (2022) ⁷⁷	CNN (ResNet18)	MIL	H&E		X	X		872		C-index	0.738
Chen et al. (2022) ⁵¹	CNN (VGG19)	ROIs	H&E, omics	Intermediate	X	X		769	1505*	C-index	0.826
Chunduru et al. (2022) ⁷⁸	CNN (ResNet50)	ROIs	H&E, omics, clinical	Late	X	X		766	1061	C-index	0.840
Braman et al. (2021) ⁸¹	CNN (VGG19)	ROIs	H&E, omics, clinical, MRI	Intermediate	X	X		176	372*	C-index	0.788
Chen et al. (2021) ⁶⁹	CNN (ResNet50)	MIL	H&E, omics	Intermediate	X	X		1011		C-index	0.817
Chen et al. (2021) ⁷⁵	CNN (ResNet50)	MIL	H&E		X	X		1011		C-index	0.824
Jiang et al. (2021) ⁵⁸	CNN (ResNet18)	WSL	H&E, omics, clinical	Early		X		490	843	C-index	0.792
Hao et al. (2019) ¹⁰³	CNN	WSL	H&E, omics, clinical	Late	X			447		C-index	0.702
Rathore et al. (2019) ¹⁰⁸	CNN (ResNet)	ROIs	H&E		X	X		663		C-index	0.820
Tang et al. (2019) ¹¹⁰	Capsule network	WSL	H&E		X			209	424	C-index	0.670
Li et al. (2018) ⁷⁴	CNN (VGG16)	MIL	H&E		X			365	491	C-index	0.622

Mobadersany et al. (2018) ⁷⁹	CNN (VGG19)	ROIs	H&E, omics	Late	X	X		769	1061*	C-index	0.801
Nalisnik et al. (2017) ⁶¹	Handcrafted		H&E, clinical	Late		X			781	C-index	0.780
Zhu et al. (2017) ⁷⁰	CNN	WSL	H&E		X			126	255	C-index	0.645
Survival time distribution modeling											
Liu et al. (2022) ¹¹¹	CNN (ResNet50)	MIL	H&E			X		486	836	C-index	0.642
Risk group classification											
Baheti et al. (2023) ⁶³	CNN (ResNet50)	MIL	H&E, omics, clinical	Late	X	X		188	188	AUC	0.746
Shirazi et al. (2020) ⁶⁶	CNN (Inception)	ROIs	H&E		X	X	X	454	858*	AUC	1.0
Zhang et al. (2020) ⁶⁴	Handcrafted		H&E, omics, clinical	Late	X			606	1194	AUC	0.932
Powell et al. (2017) ⁶⁵	Handcrafted		H&E, omics, clinical	Early		X		53		AUC	0.890
Pan-cancer studies											
Arslan et al. (2022) ⁵⁴	Autoencoder (ResNet34)	WSL	H&E		X	X		705	1489		
Chen et al. (2022) ⁸⁰	CNN (ResNet50)	MIL	H&E, omics	Intermediate		X		479		C-index	0.808
Cheerla et al. (2019) ⁹³	CNN (SqueezeNet)	SSL	H&E, omics, clinical	Intermediate		X				C-index	0.850

Table 4: Overview of all studies related to survival prediction. Studies are organized into specific subtasks and sorted by year of publication. Columns “TCGA-GBM”, “TCGA-LGG” and “Other” indicate whether TCGA-GBM, TCGA-LGG and/or other public or proprietary datasets were employed. “#Patients” and “#WSIs” state the reported size of the dataset including subsets for training and validation. “Performance” states a selection of the reported performance metrics. CNN = convolutional neural network, ROI = region of interest, WSL = weakly-supervised learning, SSL = self-supervised learning, MIL = multiple-instance learning, H&E = hematoxylin and eosin staining, MRI = magnetic resonance imaging, C-index = concordance index, AUC = area under the operator receiver curve, * = not WSIs but ROIs, ** = not gigapixel size WSIs but smaller images.